FRACTAL CHARACTERIZATION OF CAVITATION DAMAGE OF CARBURIZED AISI 5117 STEEL

B. Saleh [1, *], Tawfeeq A. Alkanhal [2], and S. M. Ahmed [3]

[1]Mechanical Eng Department, Faculty of Engineering, Assiut University, Assiut, Egypt
[2]Research Center Director of Engineering and Applied Science, Faculty of Engineering, Majmaah University, Saudi Arabia, E-mail: t.alkanhal@mu.edu.sa
[3]Mechanical Engineering Department, Faculty of Engineering, Majmaah University, Saudi Arabia, E-mail: shemy2007@yahoo.com

Received 8 January 2013; accepted 26 January 2013

ABSTRACT

The cavitation erosion of carburized and untreated low alloy steel (AISI 5117) has been investigated during the incubation period. Scanning electron microscope images of eroded surface were obtained, forming a data base for further analysis. It has been shown that carburizing can effectively improve the cavitation erosion resistance of AISI 5117 low alloy steel and prolong the incubation period. The fractal dimension and Fourier intercept values can be used to characterize the cavitation damage. The fractal dimension and Fourier intercept value for the untreated surfaces were higher than that of the carburized surfaces.

Keywords: cavitation erosion, carburizing, image analysis, AISI 5117 steel.

1. Introduction

Cavitation is defined by the ASTM standard [1] as the formation and subsequent collapse of cavities or bubbles that contain vapor or mixture of vapor and gas within a liquid. In general, cavitation originates from a local decrease in hydrostatic pressure in the liquid produced by motion of the liquid or of the solid boundary. Cavitation erosion is one of the major problems confronting the designers and users of modern high-speed hydrodynamic systems as reported by Hammitt [2]. It is a serious problem in hydraulic turbines, pumps, valves, control devices, hydraulic structures, sluices, energy dissipators, ship propellers, hydrofoils, bearings, diesel engine wet cylinder liners, aircraft engines, sonar domes, acoustic signal devices, and processing and cleaning equipment [3]. As the cavitation erosion occurs at the liquid/solid interface, it is related to surface properties rather than bulk properties. Therefore the cavitation erosion resistance of a component may be improved by some surface engineering techniques. Surface engineering techniques have the advantage of consuming only a small amount of expensive material on the surface while using an inexpensive substrate for the bulk. Therefore, researches on surface engineering techniques and coating materials are emphasized for enhancing the cavitation erosion resistance of mechanical parts in the recent years [4].

* Corresponding author.
E-mail: bahaa_saleh69@yahoo.com

To improve surface properties, it is possible to create hard, wear and corrosion resistant coatings by carburizing [5]. Using carburizing it is possible to increase parts lifetime, reliability and safety. Carburizing is the addition of carbon to the surface of low-carbon steels at temperatures (generally between 850 and 950 °C) at which austenite, with its high solubility for carbon, is the stable crystal structure. Hardening is accomplished when the high-carbon surface layer is quenched to form martensite so that a high-carbon martensitic case with good wear and fatigue resistance is superimposed on a tough, low-carbon steel core. Of the various diffusion methods pack carburizing is one of the most widely used surface hardening processes. This method has the following advantages: ease of operation; adaptability and portability of its equipment; ability to heat-treat a component after surface-finishing (since there is little oxidation, decarburization or distortion); and the ease of producing deeper zones of case depth.

Low-carbon or low-alloy steels (such as AISI 5117 steels) are used for machine elements such as cam shafts, gears and other power transmission elements after surface treatment by carburizing or nitriding. It has been shown [6-8] that, carburizing has improved the tribological properties of low carbon steel. However, the cavitation erosion of carburizing steel has not received much attention [9].

Detection and monitoring of wear are rather important in tribological researches [10, 11] as well as in industrial applications. Some typical examples are: measurement of dynamics of wear processes, engineering surface inspection, coating failure detection, tool wear monitoring and so on. With wide and extensive use of wear resistant materials, wear becomes negligibly small in some precision application down to nanometer scale. Accordingly new techniques, methodologies, and instruments for detecting or monitoring of micro-wear are increasingly demanded. Also, as a result of the dynamic and complex nature of wear process, measurement of wear is usually conducted offline and online. Consequently, detection and monitoring of wear remain challenges for tribological researches.

The objective of the present work is to use fractal analysis to assess the degree of cavitation erosion for carburized and un-carburized low carbon alloy steel. The dependence of the fractal value on the image magnification is also examined.

2. Fractal analysis

Fractal is a term introduced by Mandelbrot [12] to describe the shape and appearance of objects that have the property of self-similarity. The main concept of fractal geometry analysis is that a fractal dimension can be considered as a quantitative measure of object surface heterogeneity because of its inherent self-similarity features. In a simplified representation, one could interpret the fractal dimension as a measure of heterogeneity of a set of points on a plane, or in space. For example, when calculating the length of a coastline, the length becomes larger as the length of scale rule gets smaller. The following

numerical formula can be obtained from the fact that the length of scale rule and the coastal length are related in terms of exponential function:

$$\left(\frac{1}{\varepsilon}\right)^{D} \propto L(\varepsilon),$$

where ε is length of scale rule and L(ε) is the total measuring length. When the above expression is converted into log coordinates, the exponent D becomes the slope of the straight line. This is called power law; that is, if the compass length becomes infinitely small, the total length increases to infinite value.

From this concept, D, which can indicate the degree of complexity of length, surface, and volume, is called a fractal dimension. Fractal calculation mainly includes the calculation of profile fractal dimension $(1 < D < 2)$ and the calculation of the surface fractal dimension $(2 < D < 3)$ in tribology fractal research. Low values of D $(D \leq 2)$, indicate regularity and smoothness of surfaces, intermediate D values indicate irregular surfaces and D values close to 3 indicate highly irregular surfaces [19].

The fractal dimension of an object provides insight into how elaborate the process that generated the object might have been, since the larger the dimension the larger the numbers of degrees of freedom that are likely have been involved in that process [13]. Fractal analysis has been used to describe complex physical phenomena such as turbulence, brittle fracture of materials, machining, and tool wear [14, 15]. Fractal characterizations have also been used to describe complex two- or three-dimensional surfaces, such as deposited surfaces [16], wear-erosion surfaces [17, 18], and wear particles [19- 22]. Eroded surfaces are likely to be multifractal because they are produced by the accumulative effects of multiple impacts, i.e., rough surfaces. Fractal dimension at low frequency describes raw structures, while fractal dimension at high frequency represents texture. Textural fractal should define very fine features in the object boundary, surface, area, or volume. Structural fractal should describe an overall object morphology. Therefore, the distinction between structural and textural fractals allows investigators to characterize microstructure and macrostructure effects on the surface behavior.

Various methods have been proposed to estimate fractal values such as, Fourier, Kolmogorov, Korcak, Minkowski, root mean square, Slit Island, etc. These techniques differ in computational efficiency, numerical precision, and estimation boundary. The most efficient procedure for measurement of fractal dimension (FD) of eroded surfaces, and one which allows characterization of anisotropic surface as well, seems to be through Fourier analysis (e.g., Refs. [38, 39]). Therefore, Fourier analysis is adopted to estimate fractal values in this work. For a surface image represented by the function I(x, y), the power spectral density (PSD) is equal to the square of the Fourier transformation F(u, v) of the surface function I(x, y). The power spectral density function is defined as

$$S(u, v) = \left|F(u, v)\right|^2 \tag{1}$$

where u and v are the spatial frequencies (number of waves per unit wave length) in the x and y directions, respectively. The PSD is converted to the polar coordinate system S (f), such that $f = \sqrt{u^2 + v^2}$. The value of S(f), at each radial frequency f, is averaged over angular distributions. For a fractal surface, Fig.1(a) , the power spectrum shows a linear variation between the logarithm of S(f) and the logarithm of the frequency as shown in Fig.1(b). The slope of the linear regression line β is related to FD by the equation [23]:

$$FD = \frac{8 - \beta}{2} \tag{2}$$

It is reported in the literature that fractal dimension and intercept are significant fractal parameters that describe the irregularity and complexity of the surfaces. Moreover, the intercept correlates well with the overall magnitude of roughness of the observed texture appearance of the surface images.

(a)

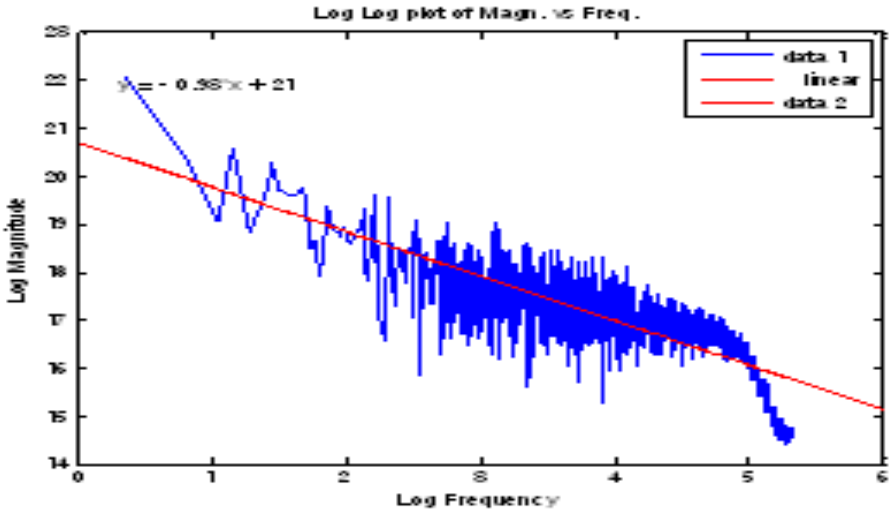

(b)

3. Experimental work

3.1. Material and heat treatment

AISI 5117 steel, (Bohler Gesellschaft, M.B.H., "Special steel" Co., Kapfenberg, Germany) in the form of rods of 16 mm diameter was selected for the study. This steel was subjected to a normalizing heat treatment process carried out by the supplier (at 850–880 °C, followed by air cooling) [24]. The nominal chemical composition and mechanical properties of AISI 5117 steel are listed in Tables 1 and 2, respectively.

Table 1

Chemical composition of low alloy steel AISI 5117 [24].

Element	C	Si	Cr	Mn	S	P	Fe
Wt. %	0.17	0.3	0.9	1.2	0.003	0.005	Balance

Table 2

Mechanical properties of low alloy steel AISI 5117 [24].

Yield Strength(MPa)	Tensile Strength (MPa)	Modulus of Elasticity (GPa)	Hardness, Hv (200 g)	Density (kg/m^3)
600	950	210	200	7850

Test specimens that have a cylindrical shape of 14 mm diameters and 10 mm height were cut from the AISI 5117 steel rod. Prior to carburizing treatment, the surfaces of specimens were polished using silicon carbide abrasive paper (grade No. 3000) to remove oxide layers and irregularities in order to enhance the uniformity of the carburized layer. The specimens were packed in a stainless steel box filled with charcoal powder (carburizing agent) with 10 % of calcium carbonate to prevent caking. The box was first filled with the carburizer compound, about 20 mm thick, and then rammed flat. The specimens were placed about 25 mm away from the sides of the carburizing box and then covered with a plate. The container was then introduced into the muffle furnace maintained at the required carburization temperature of 950°C and kept there for 6 hours followed by quenching in salt water, i.e. the hardening was effected immediately after carburization. All the carburized specimens were tempered at 200 °C for one hour. Some of the treated specimens were sectioned, polished and etched with 2 % nital solution for microstructure examination. Vickers microhardness was conducted using a Highwood HWDM-3 (TTS Unlimited Inc., Japan) instrument at a load of 200 g. The micro-hardness profile was done using sample cross-sections. The surface roughness plays an important role in developing the erosion and the material removal [25, 26]. Therefore, the specimen's working faces were polished with SiC paper successively down to 4000 grit. Before and after each test, the specimens were rinsed in acetone and dried in air and weighed with a 100 g ± 0.1 mg sensitivity balance. The eroded surface was inspected by a scanning electron microscope (SEM). The results reported below, in most cases, are the average of results obtained from tests on two specimens.

Cavitation damage tests were carried out using an ultrasonic vibratory facility conforming to ASTM standard G32-06 [27] with the stationary specimen method. A schematic diagram of the test rig is shown in Fig. 2. The peak-to-peak amplitude and the vibratory frequency used were 50 μm and 19.5 ±0.5 kHz, respectively. The specimen was placed co-axially with the horn tip held stationary at the distance L from the horn tip as shown in Fig.2. The separation distance, L, between the stationary specimen and the horn tip was initially adjusted using a dial gauge at a value of 0.8 mm to obtain a significant value of erosion [28].

Distilled water with a pH of about 7.5 was used as a cavitating liquid. The specimen and the end of the horn tip were immersed in 1200 ml open beaker, made of stainless steel, in which 700 ml of distilled water was contained. Since the test liquid temperature markedly affects the degree of erosion [29,30], the test water temperature in the beaker was controlled by cooling water circulating around and was always maintained at 24±1 °C , as shown in Fig.2. Preliminary tests showed that temperature of the liquid film on the specimen surface rose rapidly regardless of the constant temperature in the beaker. This temperature was measured for a maximum duration test time with a thermocouple inserted in the center of test piece. It was taken into account that the insertion of thermocouple has no effect on the film thickness. It was found for 10 min. (maximum interval test time), that the film temperature did not exceed the controlled temperature of beaker by more than 2C.

4. Results and discussion

4.1. Morphology and hardness of carburized steel

When the material (AISI 5117 steel) was examined, it was seen that the microstructure composed of proeutectoid - α phase (white areas in Fig. 3) and fine pearlite micro-constituent (α + Fe_3C) (dark areas in Fig. 3). After carburizing, the microstructures of specimens have been examined and the following conclusions have been drawn. The micrograph of sample shown in Fig. 4 shows that the case depth attains approximately 0.65 mm. The microstructure near the surface is almost completely martensitic due to the high carbon content and again small amount of retained austenite can be seen as well (Fig. 3).

Hardness measurements of the specimens were done before and after the heat treatment on a straight line from the surface to the core as shown in Fig. 5. The hardness of the untreated specimen is 200 HV and is constant with depth. The hardness of treated specimen at or near the surface attains a value of approximately of 930 HV. It then decreases gradually with the depth and reaches a constant value about 430 HV at the core.

4.2. Eroded surface topography

4.2.1. Untreated specimens

Figures 6 and 7 show the damage developed on the specimens surfaces of untreated steel after cavitating for test time of 15, 30, 45, 60, and 75 min. for low and high magnification, respectively. Eroded surface topography for t =15 min, shown in Fig.6. illustrates that there are three distinct features of damage, namely: corrosion pits, cavitation pits and slip bands. The characteristic feature of the corrosion pit is the presence of two parts: cavity at the pit center and a rough circular band or ring area, which is labeled 1 in Fig. 6. Some of these pits appear to be individuals and the others to be overlapping. The circular band size may reach to 40 µm. These circular bands around the corrosion pits represent the corrosion products. The same features for these corrosion pit has been observed before in the literature on cavitation erosion on 1045 carbon steel [31, 32].

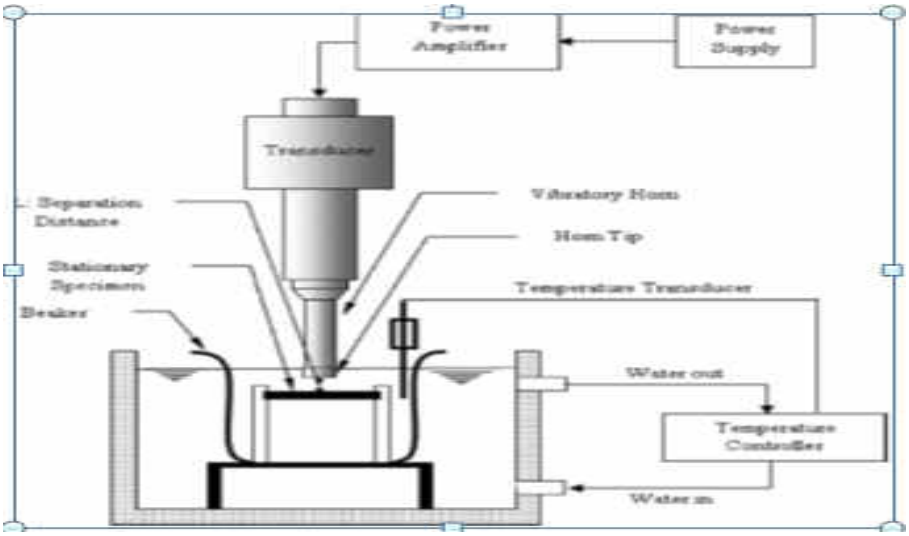

Fig. 2. Schematic view of the test apparatus

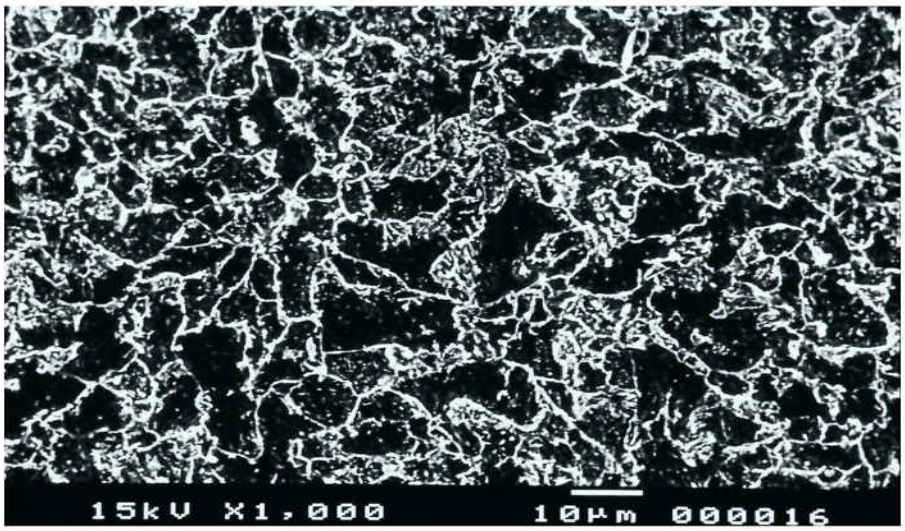

Fig. 3. SEM microphotograph of 5117 steel microstructure**.**

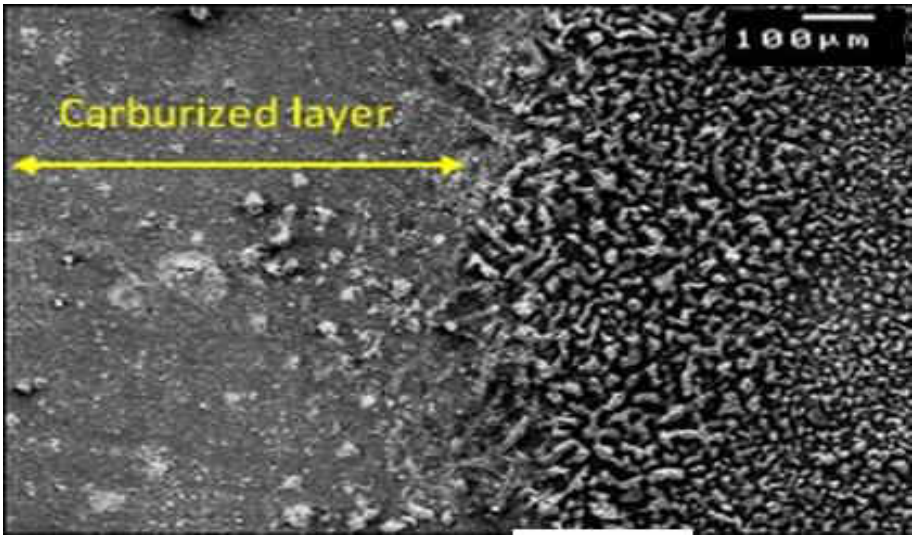

Fig. 4. SEM micrographs showing microstructures of carburized case depth after 6 h

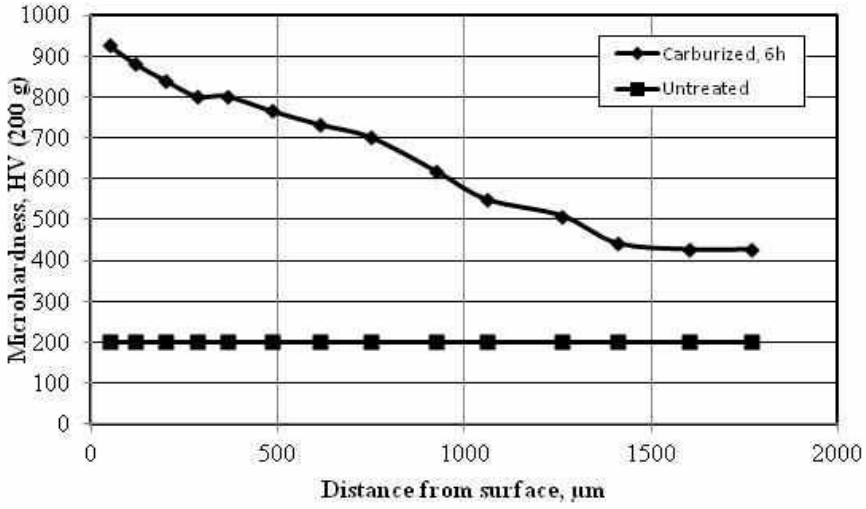

Fig. 5. Hardness distribution of treated and untreated material**.**

The cavitation pits, which are labeled 2 in Fig. 6, are few in number and small in size. They have an irregular shape. The maximum size of cavitation erosion pits is of order 2 μm. Such a tiny pit cannot be successfully described by the shock wave. It is therefore clear that it arises from highly erosive microjet impact of stress larger than the strength of the tested materials.

It can be seen in Fig. 6, that there are numerous small white areas which have a longitudinal shape. These areas differ from the large ones which are classified as

corrosion pits. They are classified as slip bands. These slip bands can be seen from Fig. 6 at t = 15 min. at high magnification.

The development of erosion and the role of corrosion pits, cavitation pits and plastic deformation can be revealed from photos for t = 30-75 min. in Figs. 6 and 7. It can be seen that the surface suffered from severe plastic deformation. It can also be observed that many holes of relatively large sizes are formed and many cracks have been developed at t = 30 min. The formation of the holes is attributed to the coalescence of the voids in material due to plastic deformation [33], and not to the particle dislodged off and not to the joining of pits. This was verified by trying to collect the particle debris after the test using the magnetic technique [34], and no particles were observed by SEM observation. In previous works, some of the authors have observed that the pit size does not change with the time and their number decreases also with the time [26, 35]. In the light of the eroded surface morphology [25, 26, 33, 35], the feature morphology of particle debris [30, 34] and the cavitation bubble behavior, it can be concluded that the microjet pits scarcely play an important role on the erosion accompanied with considerable amount of mass loss. It is worth to be noted that the corrosion pits disappear for t = 30 min. This means that the corrosion effect in developing the severe damage in such case may be negligible.

The initial surface roughness of the surface plays an important role in developing the erosion. This can be revealed from Fig. 7 at t = 30 and 45 min., where it can be seen that many cracks nucleated and propagated along the traces of polishing lines. This is due to the fact that the surface roughness represents one of the origins of the stress concentration. In previous investigation by one of the authors [23, 24, 35, 36], it was found that the initial roughness, even when it was very small (maximum roughness height, R_{max} = 25 nm), it not only acts as weak spots for gathering the pits [26] that develop to microcracks [25], but also accelerates the crack propagation and the material removal [36]. It was also observed that the initial surface roughness facilitates the fall-off particles, especially the longitudinal one [37]. This is also clear in photo at t =45 min. in Fig. 7, where many longitudinal particles in the bottom part of the photo developed. With increasing the exposure time, many particles have fallen-off as in Fig. 7 at t = 60 min., but there is no detectable weight loss. At t = 75 min., the material removal become detectable and it was 0.8 mg.

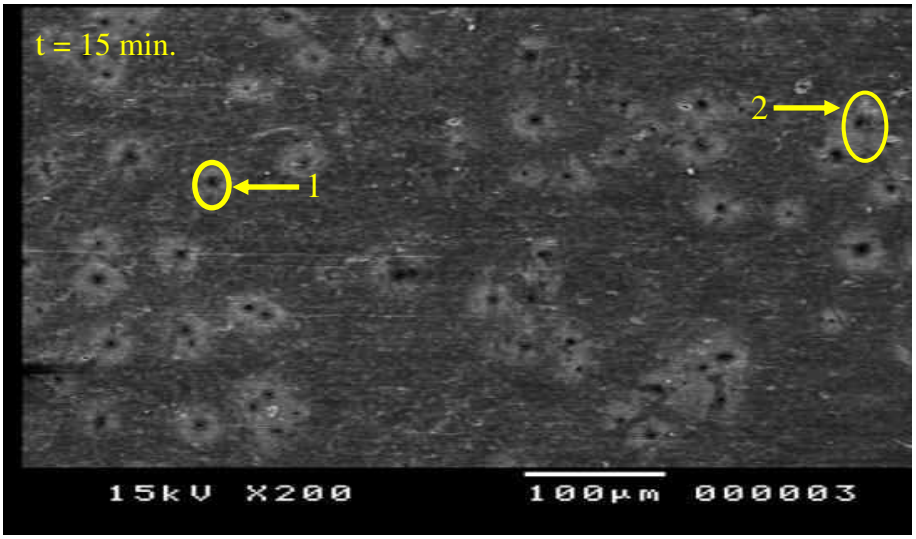
t = 15 min.
1
2
15kV X200
100µm 000003

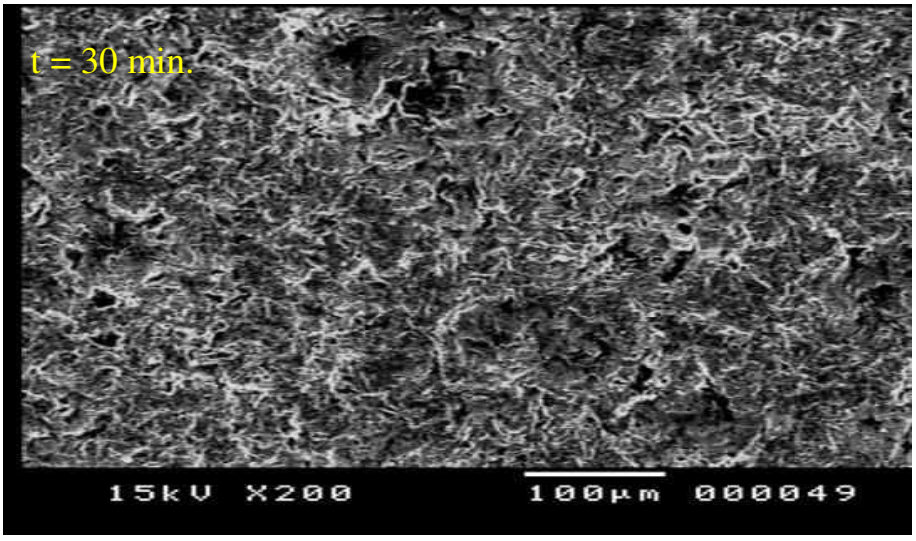
t = 30 min.
15kV X200
100µm 000049

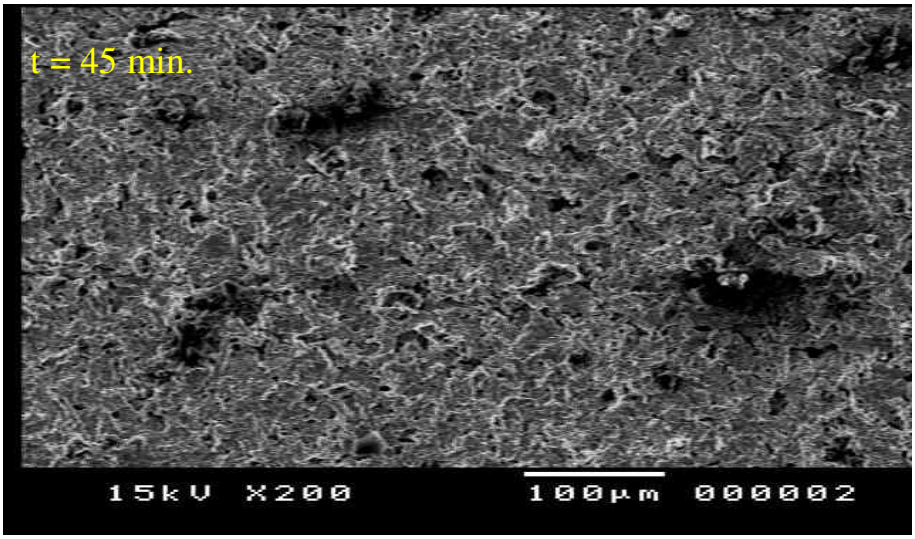
t = 45 min.
15kV X200
100µm 000002

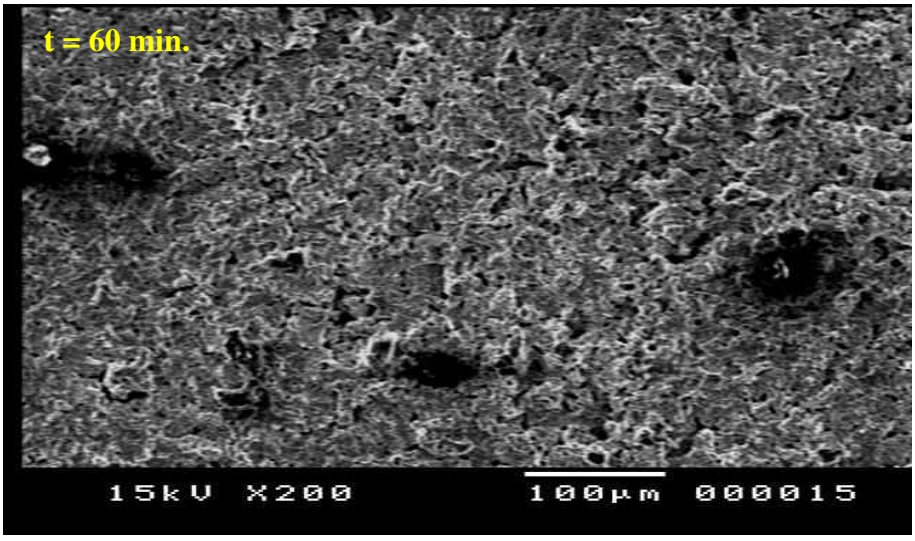
t = 60 min.
15kV X200
100µm 000015

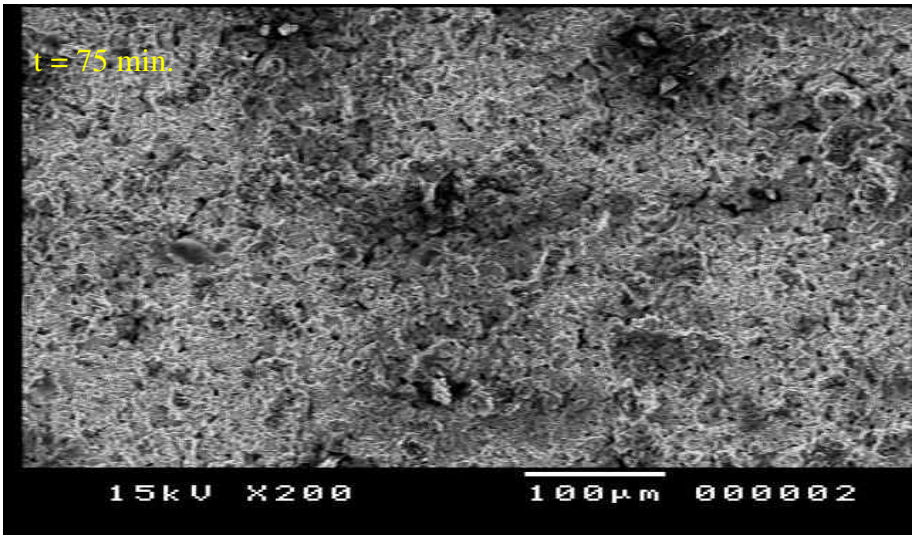

Fig.6. SEM photographs of eroded surfaces for untreated steel at low magnification for t = 15, 30, 45, 60, and 75 min. respectively

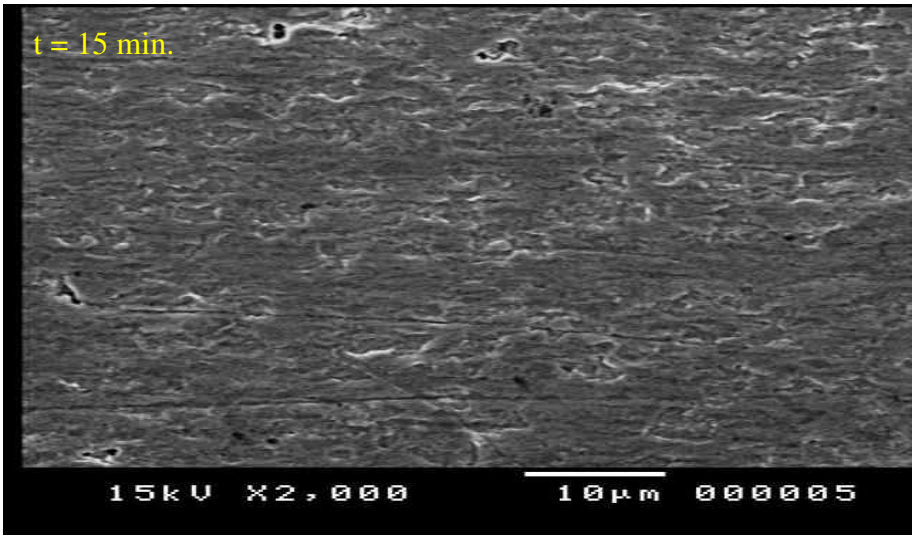

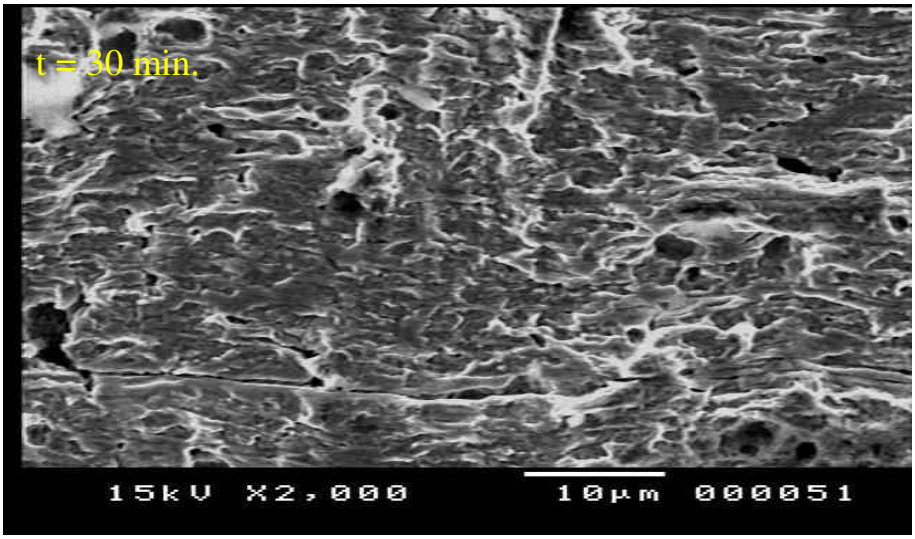
t = 30 min.
15kV X2,000 10µm 000051

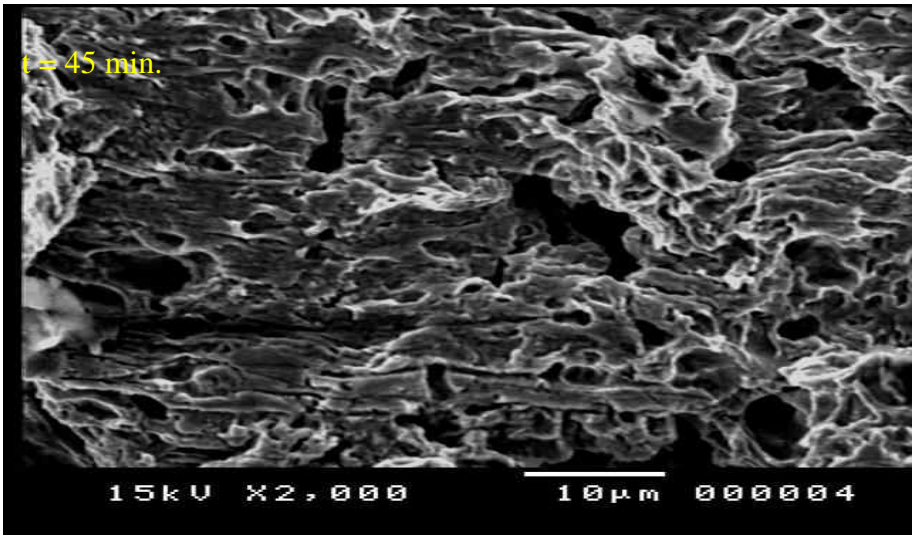
t = 45 min.
15kV X2,000 10µm 000004

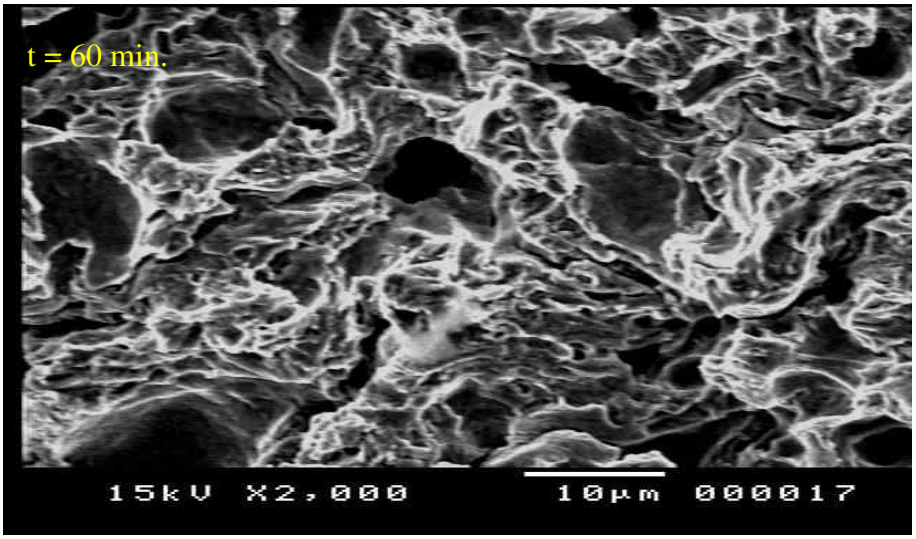

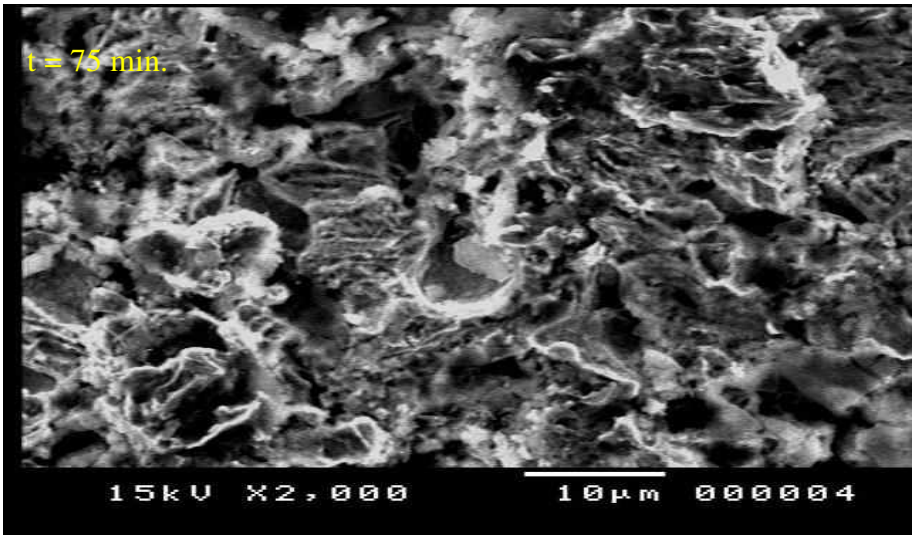

Fig.7. SEM photographs of eroded surfaces for untreated steel at high magnification for t = 15, 30, 45, 60, and 75 min. respectively

4.2.2. Carburized steel specimens

The surfaces of carburized steel specimens which were exposed to cavitation erosion at t = 15, 30, 45, 60, 75 min. are depicted in Figs 8 and 9. By examining the eroded surfaces for low and high magnifications, it was difficult to find any features for cavitation damage except some few indentations or pits randomly distributed and delineation of polishing traces. This proves that carburization is effective in prolonging the incubation period. Therefore, carburization and its effectiveness on the development of erosion will be treated in detail in future.

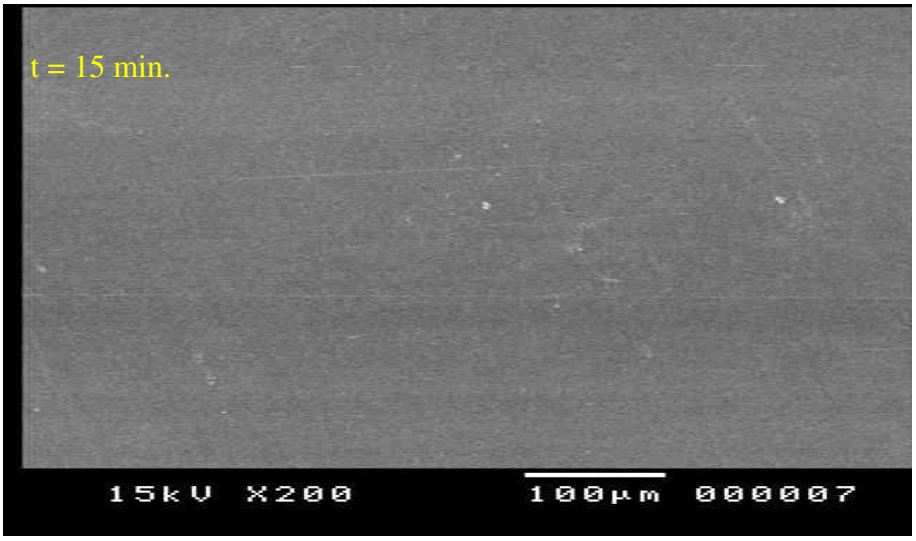

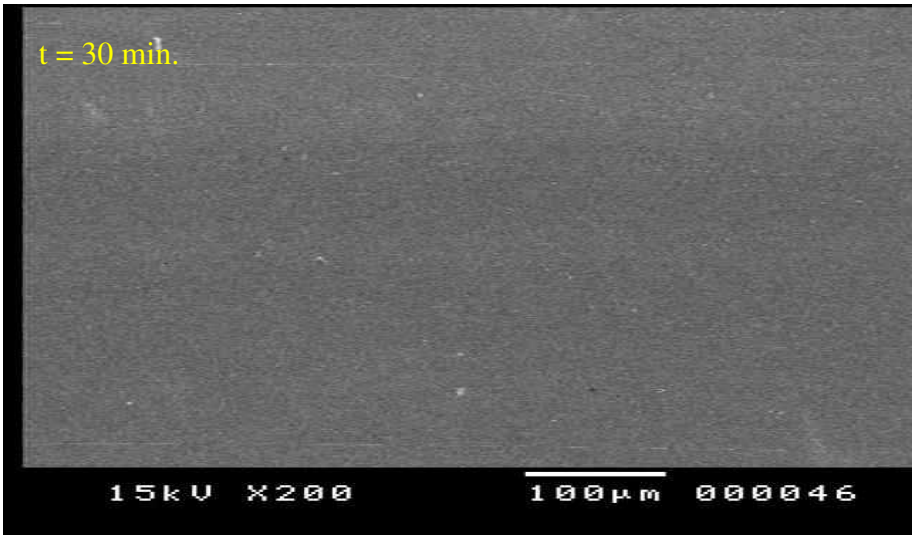
t = 30 mih.
15kV X200
100µm 000046

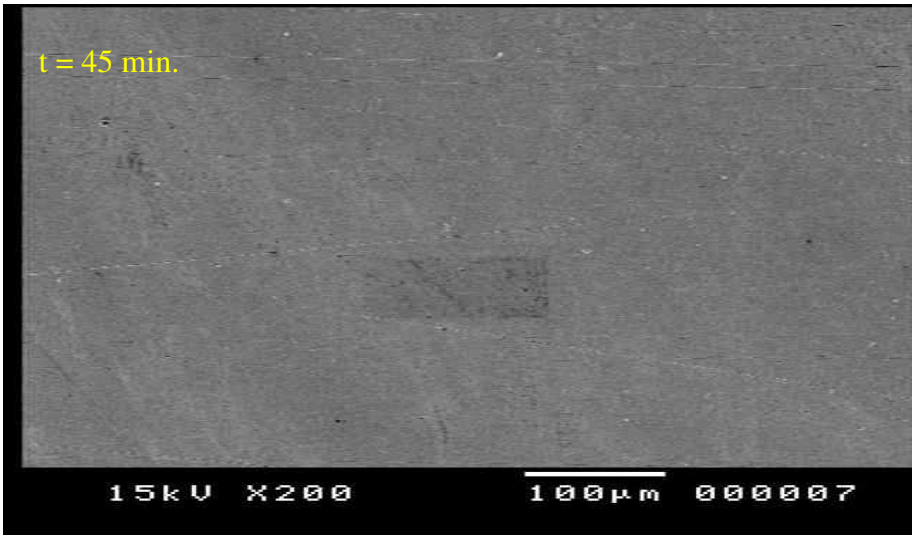
t = 45 min.
15kV X200
100µm 000007

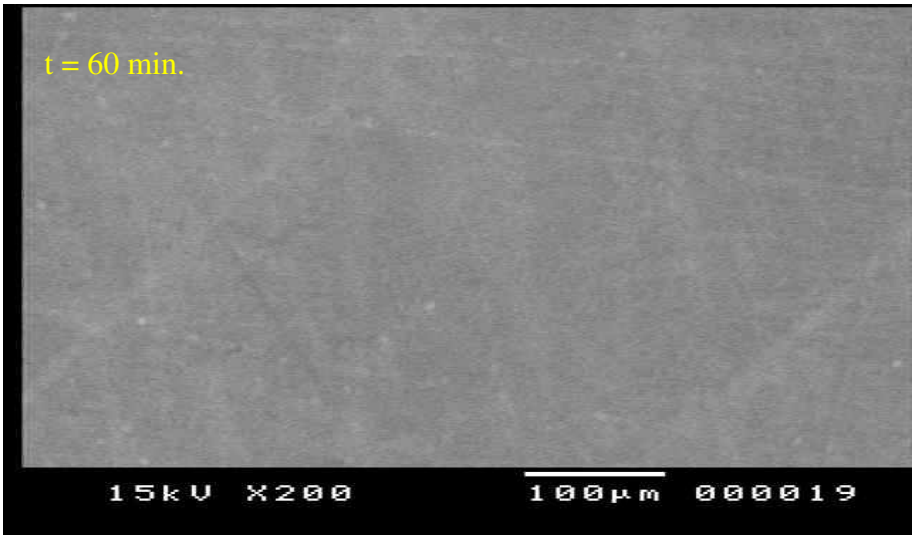

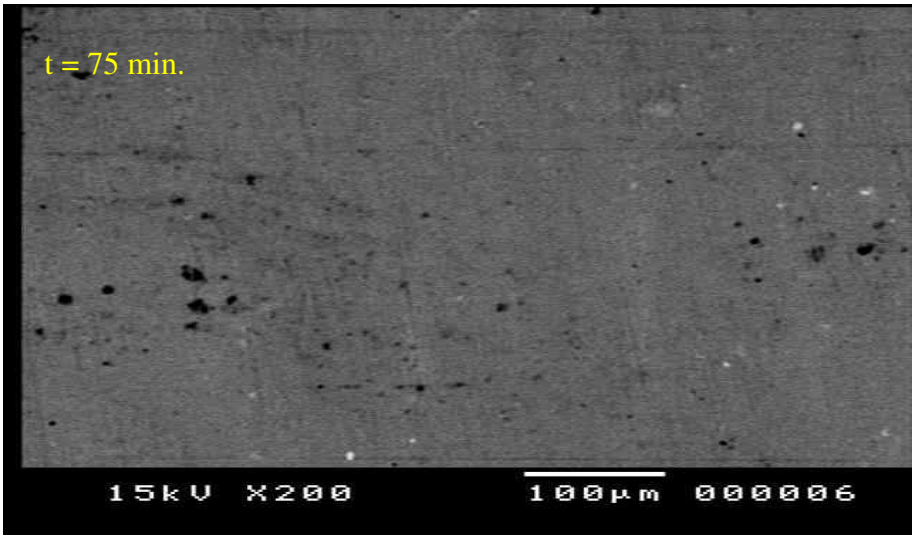

Fig.8. SEM photographs of eroded surfaces for treated steel at low magnification for t = 15, 30, 45, 60, and 75 min. respectively

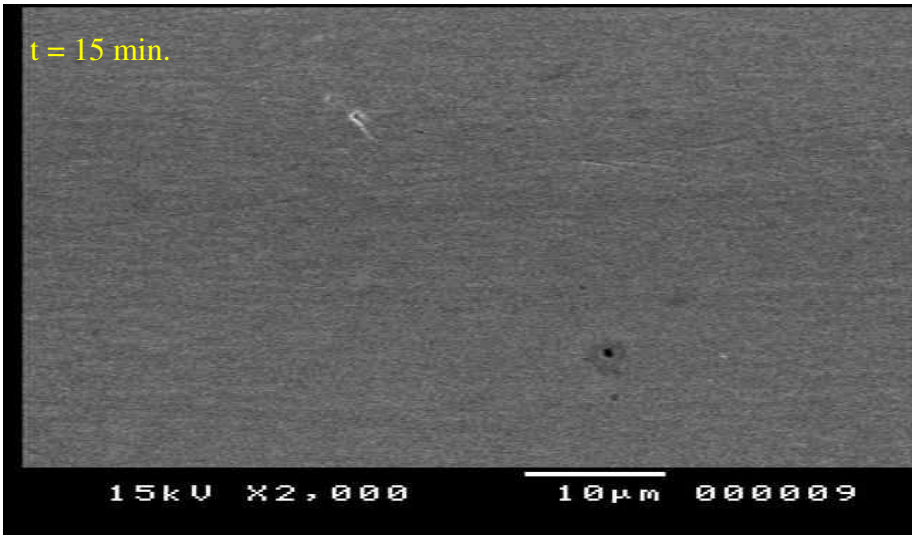
t = 15 min.
15kV X2,000 10µm 000009

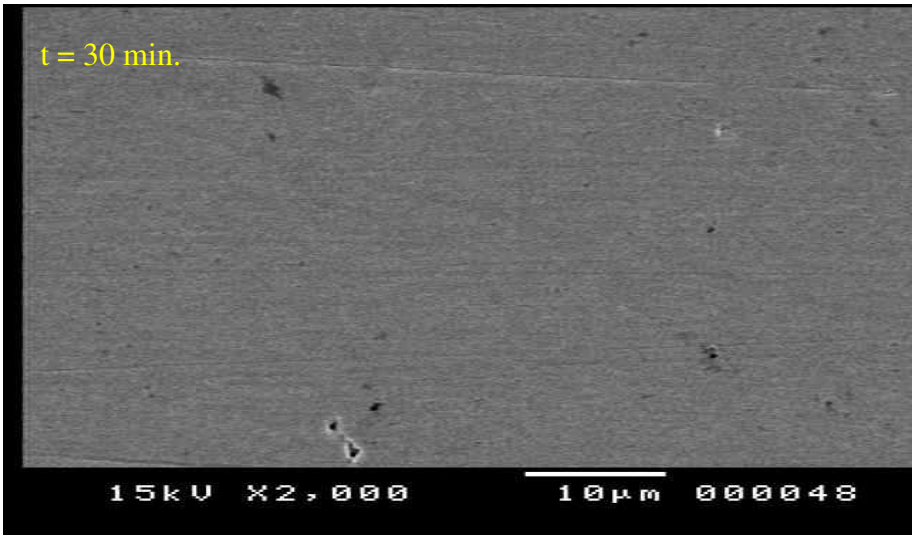
t = 30 min.
15kV X2,000 10µm 000048

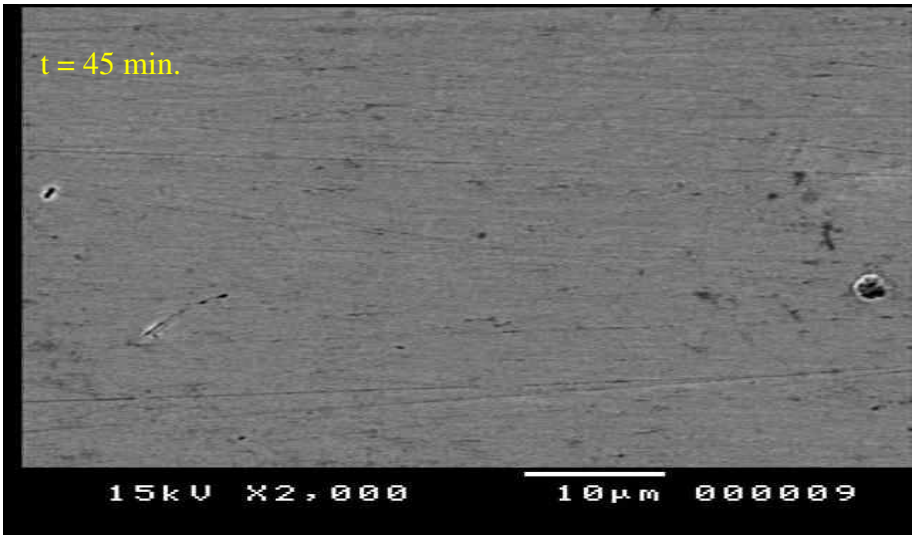
t = 45 min.
15kV X2,000 10µm 000009


t = 60 min.
15kV X2,000 10µm 000021

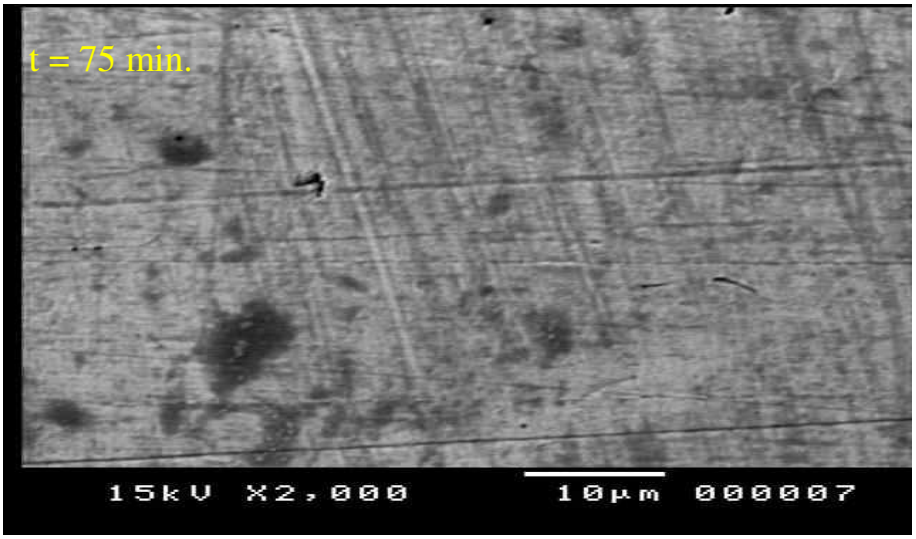

Fig.9. SEM photographs of eroded surfaces for treated steel at high magnification for t = 15, 30, 45, 60, and 75 min. respectively

4.3. Fractal characteristics of surface damage

To investigate the possibility of application of fractal analysis to detect the degree of damage for untreated and carburized specimens, the fractal dimension and Fourier intercept values are measured for the eroded surfaces with the test time. Because fractals determined in this study are not a measure of special dimensions but rather of variation in structure, or more properly, variations in the gray scale of micrographs, fractal determined from micrograph will be referred to as fractal values [18]. In this case, the fractal values are the slope of fitted lines, as shown in Fig. 1. The results are shown in Figs. 10 and 11. Figs. 10 and 11 illustrate the fractal dimension and intercept values versus the time for treated and untreated eroded surfaces at magnifications of 200 (a) and 2000 (b), respectively, Both the fractal dimension and the intercept change with the time, However the change in the data for the untreated surface fluctuates with the time for low magnification. Generally, it can be observed that fractal dimension and intercept steadily increase with time for treated surfaces. From these figures, it can be seen that fractal dimension and intercept values for untreated specimen are higher than that for treated specimens. This is in consistence with the appearance of the eroded surface topography, where the untreated specimen has been severely plastically deformed and the treated specimen still resists the deformation. However the difference in fractal values for treated and untreated surfaces are remarkable for $t < 75$ min. while at $t = 75$ min. the difference is negligibly small.

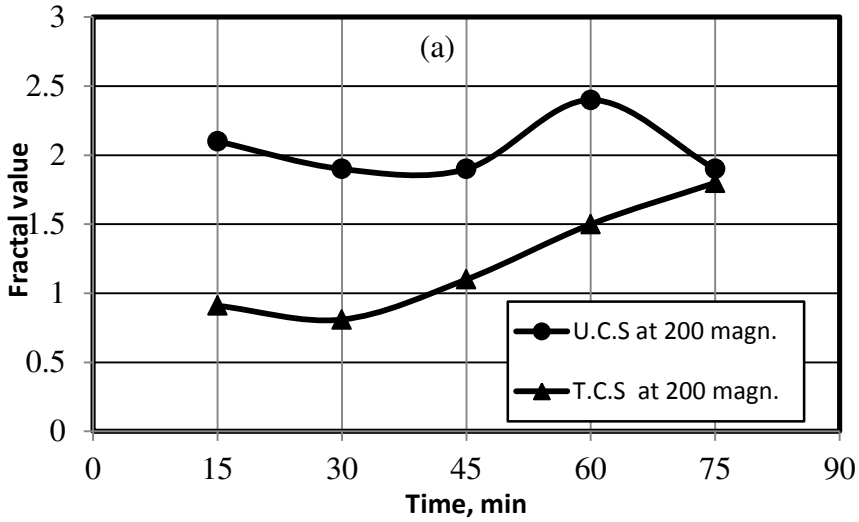

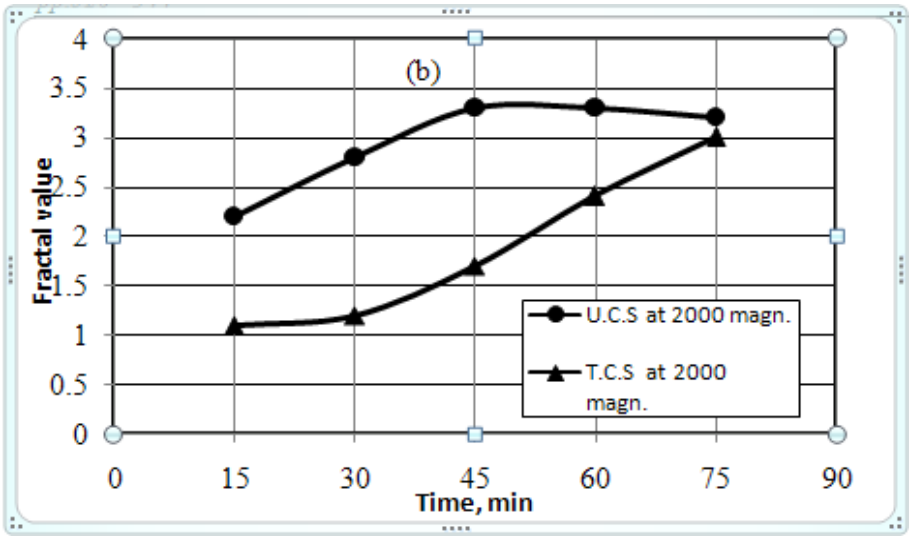

(b)

Fig. 10. Variation of fractal dimension versus time for treated and untreated surfaces at (a) low magnification and at (b) high magnification.

(a)

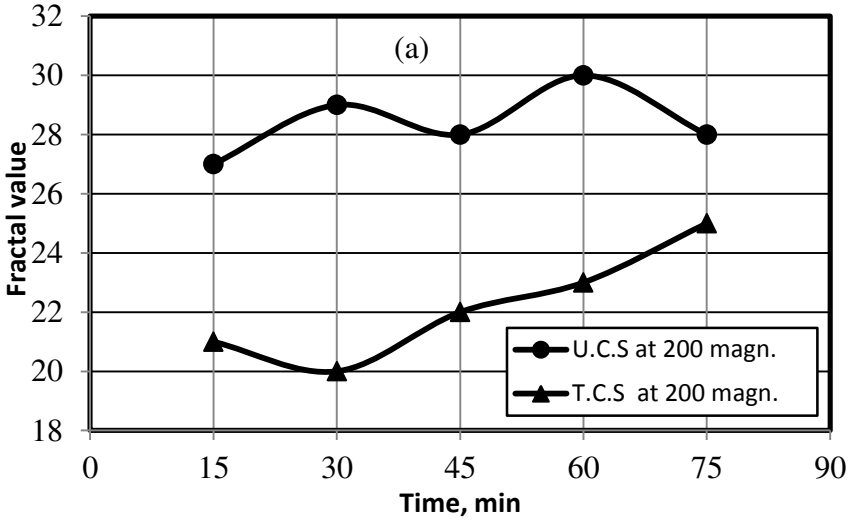

(b)

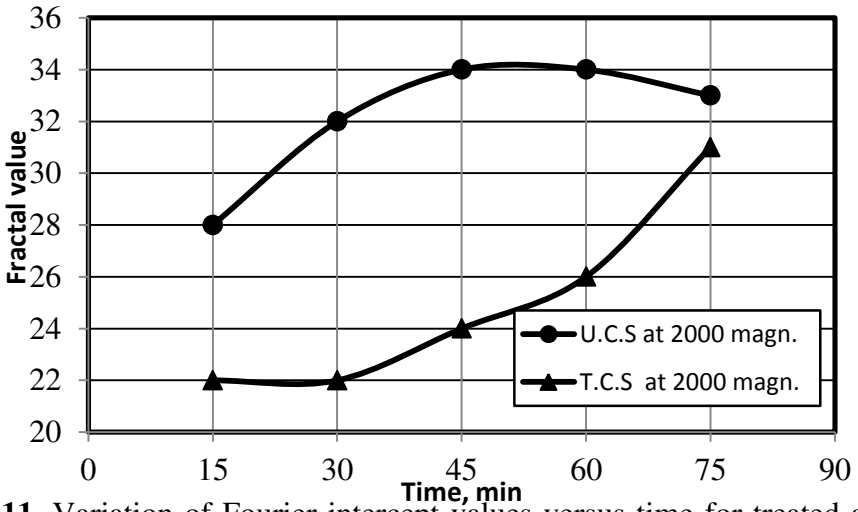

Fig. 11. Variation of Fourier intercept values versus time for treated and untreated surfaces at (a) low magnification and at (b) high magnification.

This investigation confirmed the usefulness of the Fourier analysis dimension and Fourier intercept as quantitative descriptors of visual texture in eroded surface images [38, 39].

5. Conclusions

In this investigation, the cavitation damage behaviour of untreated and carburized AISI 5117 steel has been examined at incubation period. The main conclusions from this investigation can be summarized as follows:

1- Carburizing of AISI 5117 low carbon alloy steel specimens shows a higher cavitation erosion resistance than the untreated specimens as well as increase of the incubation period.
2- The fractal analysis can be used to characterize the surface topography of cavitation damaged surfaces.
3- The fractal dimension and Fourier intercept values vary with time and their values for the untreated surfaces are higher than that for carburized ones.

References

[1] ASTM Designation, G32-06, Standard test method for cavitation erosion using vibratory apparatus, Annual Book of ASTM standard, pp. 98-112, 2006.
[2] Hammitt, F. G., "Cavitation Erosion: The State of The Art and Predicting Capability", Appl. Mech. Rev., 32, 6, pp. 665-675, 1979.
[3] Preece, C. M., "Cavitation Erosion", Treatise on Materials Science and Technology, C. M. Preece, ed., Erosion Academic, New York, 16, pp. 249, 1979.
[4] DING Zhang-xiong1, CHEN Wei1, and WANG Qun, "Resistance of cavitation erosion of multimodal WC-12Co coatings sprayed by HVOF", Trans. Nonferrous Met. Soc. China, 21, pp. 2231−2236, 2011.
[5] Kennedy, D. M., Xue, Y., and Mihaylova, E., "Current and Future Applications of Surface Engineering", The Engineers Journal (Technical) 59, pp. 287-292, 2005.
[6] Selcuk, B., Ipek, R., and Karamis, M. B., "A Study on Friction and Wear Behavior of Carborized Carbonitridid and Borided AISI 1020 and 5115 Steels", J. Mater. Process. Technol., 141, pp. 189-196, 2003.
[7] Patel, S. K., and Kumar, M., "Erosive Wear Characteristics of Carburized Mild Steel in Soil-Water Slurry", Proc. of the 4th International Conference on Advances in Mechanical Engineering, S.V. National Institute of Technology, Surat-395 007, Gujarat, India. September 23-25 pp. 1-5, 2010.
[8] Gupta, J., "Mechanical and Near Properties of Carburized Mild Steel Samples", Master thesis, Dep. of Mech .Eng., National Inst. Of Techn., Rourkela, India, 2009.
[9] Dojcinovic, M., and Markovic, S., "The Morphology of Cavitation Damage of Heat-Treated Medium Carbon Steel", J. Serb. Chem. Soc., 71 (8-9), pp. 977-984, 2006.
[10] Zhang, J., "Detection and Monitoring of Wear Using Imaging Methods", Ph. D. thesis, University of Twente, Enschede, Netherlands, 2006.
[11] Saridakis, K. M., Nikolakopoulos, P. G., Papadopoulos, C. A., and Dentsoras, A. J. "Fault Diagnosis of Journal Bearings Based on Artificial Neural Networks and Measurements of Bearing Performance Characteristics", in B.H.V. Topping, M. Papadrakakis, (Editors), Proceedings of the Ninth International Conference on Computational Structures Technology,

Civil-Comp Press, Stirlingshire, UK, Paper 118, doi:10.4203/ccp.88.118, 2008.

[12] Mandelbrot, B. B., "The Fractal Geometry of Nature", W.H. Freeman and Company, New York, 1983.

[13] Klonowski, W., "Signal and Image Analysis Using Chaos Theory and Fractal Geometry", Machine Graphics & Vision, 9, pp. 403-431, 2004.

[14] Russ, J. C., "Fractal Surfaces", Plenum, New York, 1994.

[15] Kassim, A. A., Zhu, M., and Mannan, M. A., "Texture Analysis Using Fractals for Tool Wear Monitoring", IEEE ICIP, pp. III-105–III-108, 2002.

[16] Guessasma, S., Montavon, G., and Coddet, C., "On the Implementation of the Fractal Concept to Quantity Thermal Spray Deposit Surface characteristics", Surf. Coat. Technol., 173(1), pp. 24-38, 2003.

[17] Ribeiro, L. M. F., Horovistiz, A. L., Jesuino, G. A., Hein, L. R., de, O. Abdade, N. P., and Crnkovic, S. J., "Fractal Analysis of Eroded Surfaces by Digital Image Processing", Mater. Lett., 56, pp. 512-517, 2002.

[18] Rawers, J., and Tylczak, J., "Fractal Characterization of Wear-Erosion Surfaces", J. Mater. Eng. Perform, 8(6), pp. 669-676, 1999.

[19] Yuan, C. Q., Li, J., Yan, X. P., and Peng, Z., "The Use of the Fractal Description to Characterize Engineering Surfaces and Wear Particles", Wear, 255, pp. 315-326, 2003.

[20] Stachowiak, G. W., and Podsiadlo, P., "Characterization and Classification of Wear Particles and Surfaces", Wear, 249, pp. 194-200, 2001.

[21] Podsiadlo, P., and Stachowiak, G. W., "Scale-Invariant Analysis of Wear Particle Morphology: A Preliminary Study", Tribol. Int., 33, pp. 289-295, 2000.

[22] Stachowiak, G. W., "Numerical Characterization of Wear Particles Morphology and Angularity of Particles and Surfaces", Tribol. Int., 31(1-3), pp. 139-157, 1998.

[23] Costa, M. A., "Fractal Description of Rough Surfaces for Haptic Display", Ph. D. thesis, Stanford University, Stanford, CA, 2000.

[24] Bohler, "Special Steel Manual", A-8605 Kapfenberg, Germany, 90-98, 2000.

[25] Ahmed, S. M., Hokkirigawa, K., Kikuchi, K., Matsudaira, Y., Oshima, R., and Oba, R., "Marked Surface-Roughness Effects on the Development of Microfracture During the Incubation Period of Vibratory Cavitation Erosion", Proceedings of the Third Japan-China Joint Conference, Osaka, Japan, Vol. I, pp. 331-338, 1990.

[26] Ahmed, S. M., Hokkirigawa, K., Ito, Y., and Oba, R., "Scanning Electron Microscopy Observation on the Incubation Period of Vibratory Cavitation Erosion", Wear, 142, pp. 303-314, 1991.

[27] ASTM G 32-09: Standard test method for cavitation erosion using vibratory apparatus. Annual book of ASTM standards, ASTM, Philadelphia, PA, 2009.

[28] Vyas, B., and Preces, C. M. "Stress Produced in a Solid by Cavitation", J. Appl. Phys., 47 (2), pp. 5133-5138, 1976.

[29] Ahmed, S. M., "Investigation of the temperature effects on induced impact pressure and cavitation erosion", Wear, 218, pp. 119-127, 1997.

[30] Saleh, B., Abouel-Kasem, A., Ezz El-Deen, A. and Ahmed, S. M., "Investigation of Temperature Effects on Cavitation Erosion Behavior Based on Analysis of Erosion Particles", Trans. ASME, J. Tribol., 132, pp. 041601 1-6, 2010.

[31] Karrab, S. A., Doheim, M. A., Mohammed, M. S., Ahmed, S. M., "Study of cavitation erosion pits on 1045 carbon steel surface in corrosive waters", ASME, J. Tribol., 134 (1), pp. 011602, 2012.

[32] Karrab, S. A., Doheim, M. A., Mohammed, M. S., Ahmed, S. M., "Investigation of the Ring Area Formed Around Cavitation Erosion Pits on the Surface of Carbon Steel", Tribology

Letter.45 (3), pp. 437-444, 2012.
[33] Ahmed, S. M., Hokkirigawa, K., and Oba, R., "Fatigue Failure of SUS 304 Caused by Vibratory Cavitation Erosion", Wear, 177, pp. 129-137, 1994.
[34] Abouel-Kasem, A., Saleh, B., Ahmed, S. M., "Quantitative Analysis of Cavitation Erosion Particle Morphology in Dilute Emulsions", Trans. ASME, J. Tribol., 130, pp. 041603 1-6, 2008.
[35] Abouel-Kasem, A., Ezz-El-Deen, A., Emara, K. M., and Ahmed, S. M., "Investigation Into Cavitation Erosion Pits", ASME J. Tribol., 131 (3), pp. 031605 1-7, 2009.
[36] Ahmed S. M. Hokkirigawa, K., Oba, R. and Kikuchi, K., "SEM Observation of Vibratory Cavitation Fracture Mode during the Incubation Period and the Small Roughness Effect", JSME Int. J., Ser. II, 34 (3), pp. 298, 1991.
[37] Ahmed, S. M., Hokkirigawa, K., Higuchi, J. and Oba, R., "SEM Studies of Particles Produced by Cavitation Erosion", JSME Int. J. Ser. B., 36, pp. 517, 1993.
[38] Abouel-Kasem, A., Alturki, F. A., and Ahmed, S. M., "Fractal Analysis of Cavitation Eroded Surface in Dilute Emulsions", Trans. ASME, J. Tribol., 133 (4), pp. 041403-12, 2011.
[39] Alturki, F. A., Abouel-Kasem, A., and Ahmed, S. M., "Characteristics of Cavitation Erosion Using Image Processing Techniques", J. Tribol. 135 (1), pp. 014502-9, 2013.

توصيف التآكل الناتج عن التكهف لسبيكة من الصلب (AISI 5117) المكربن باستخدام الهندسة الكسرية (فراكتال)

ملخص:

تم في هذا البحث دراسة التآكل الناتج عن التكهف خلال فترة الاحتضان لسبيكة من الصلب (AISI 5117) تمت معالجتها بالكربنة وأخرى غير معالجة. وباستخدام المجهر الإلكتروني ألتقطت صور للسطح المتآكل وشكلت تلك الصور قاعدة بيانات لمزيد من التحليل. ولقد أظهرت النتائج أن الكربنة يمكن أن تحسن بشكل فعال من مقاومة سبيكة الصلب (AISI 5117) للتآكل الناتج عن التكهف وتطيل عمر فترة الاحتضان. باستخدام الهندسة الكسرية (فراكتال) تم تحليل الصور عن طريق البعد الكسري وقيم التقاطع لفورير وتبين إمكانية استخدامهما لوصف الضرر الناتج عن التآكل وكان كلا من البعد الكسري وقيم التقاطع لفورير أعلى للسطوح غير المعالجة عن تلك التي للسطوح المعالجة.